Design, modeling and identification of the Generation Side Converter in an 11.7 kW wind/photovoltaic hybrid renewable generation system

João Lucas Da Silva, Geovane Luciano dos Reis, Rafael Mario da Silva, Seleme Isaac Seleme Junior, Thierry A. Meynard, Ana Maria Llor

Design, Modeling and Identification of the Generation Side Converter in an 11.7 kW Wind/Photovoltaic Hybrid Renewable Generation System

J.L. Da Silva[1,3]; G. L. Dos Reis[1,2]; R. M. Silva[1,2]; S.I. Seleme Jr[2]; T. A. Meynard[3]; A. M. Llor[3]

[1]Federal University of Itajubá
UNIFEI
Laboratory of Conversion and Control of Electric Energy,
Itabira, MG - Brazil

[2]Federal University of Minas Gerais
UFMG
Graduate Program in Electrical Engineering
Belo Horizonte, MG - Brazil

[3]University of Toulouse
Laboratory on Plasma and Conversion of Energy,
Toulouse – France

Abstract- This study focuses on the design and control of an 11.7 KW hybrid generation system using photovoltaic panels and a wind turbine. The conversion is accomplished by a multicell converter divided in two stages: the Generation Side Converter (GSC) and the Mains Side Converter (MSC). This paper will present the design of GSC highlighting the key components (wind turbine, photovoltaic cells, switching elements and passive filter), their models and parameters' identification.

Keywords–*Permanent Magnet Synchronous Generator (PMSG), Wind Turbine, Photovoltaic Panels (PV panels), Hybrid Generation, Boost Converter.*

I. INTRODUCTION

Distributed and micro-energy generation systems represent an important solution for the energetic matrix diversification in opposition to the classical centralized way of production. The first positive aspect is that the natural resource should not be abundant since the generation is in small scale. For the same reason, the implantation costs are reduced and affordable for regular citizens and not only for big companies. Among the technologies for small scale production, photovoltaic and wind energy generation have become the most promising sources due to their worldwide availability, null cost and sustainability [1].

In micro-generation, achieving a higher level of capacity factor is probably the biggest challenge since no high investments in the resource availability research can be accomplished, because this would increase deeply the total costs of implantation. In this context, hybrid systems present an important possibility for improving the system's capacity factor.

Hybrid systems are a combination of different power generation sources configured to meet specific requirements, such as reliable and low-cost electrical power [2]. The use of renewable energy sources (wind, geothermal, solar, biomass, etc.) in hybrid generation has the great advantage of allowing the sharing of system components. Another important point is that each of the power generation systems can operate separately, but when combined they provide functionality that would not be possible from just one power source, such as a complementarity, increasing the reliability of the generation system[3][4].

The configuration of a hybrid generator depends on the type of power converters used to connect the different power sources to the loads. Usually the converters applied in these systems are CA-DC, DC-CA and DC-DC, such configurations involve critical technical issues, which has attracted the attention of several researchers in the development of several works in this sense.

The 11.7kW Hybrid Renewable Generation System (HRGS) approached in this study is divided in the Generation Side Converter (GSC) and the Mains Side Converter (MSC). The models and parameter identification of these elements will be presented focusing the GSC. Initially, an overview of the HRGS will be given with the detailed description of each element, the wind generator and solar panels will be presented, their models and parameters, obtained from measurements and tests.

II. CONVERTER COMPONENTS OVERVIEW

A. Wind/Photovoltaic Hybrid Renewable Generation System (HRGS)

The Fig. 1presents the wind/photovoltaic HRGS. It contains two circuits of photovoltaic panels connected to the conversion system and a vertical axis wind turbine with permanent magnet synchronous generator (PMSG).

Each photovoltaic circuit consist of two arrays of10 panels in parallel. There are 40 panels of 255(W) performing, in total, 10.2(kW) of photovoltaic generation. The circuits are connected to boost converters that are responsible for the independent current control of each array. The boost converters present not only an input inductor but also a capacitor, performing an LC filter, in order to reduce the ripple in the output voltage of the panels. A reduced ripple in the panels' voltages is important for an operation with higher efficiency

and for guarantying a better tracking in the point of maximum power (MPPT).

The wind generation part is a vertical axis turbine attached to a 1.5(kW) three-phase permanent magnet synchronous generator (PMSG). A non-controlled rectifier is connected to the PMSG and a third boost converter controls the current flow from the generator to the DC-link. The boost input current is proportional to the electromagnetic torque and it controls the turbine speed.

The two boost converters responsible for the photovoltaic conversion (B_1 and B_2) and the wind generator's rectifier and boost (R_1 and B_3), together with the input inductors and capacitors perform the generation side converter (GSC). The GSC allows the conversion to a fixed DC-link voltage, but also guarantees the independent control for each input allowing the maximum power point tracking of the panels and wind turbine.

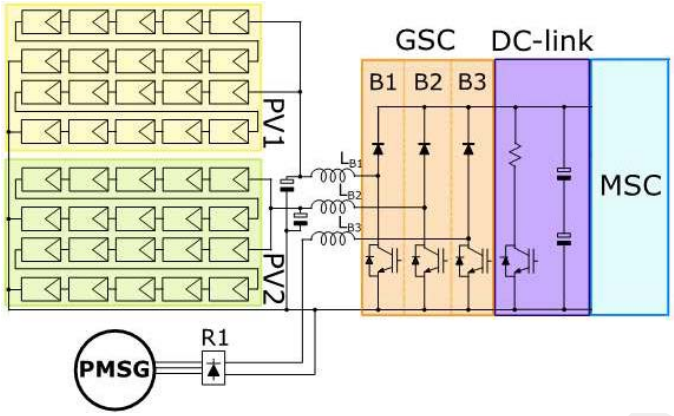

Fig. 1: Schematics of the GSC with Wind/Photovoltaic conversion system

A picture of the installation is presented in Fig. 2 highlighting the solar panels and vertical axis wind turbine.

Fig. 2: Photovoltaic panels and vertical axis turbine in the HRGS.

On the other side, the Mains Side Converter (MSC) accomplishes the connection to the grid through an LCL filter. The MSC controls the DC-link voltage and, by doing that, it allows the power flow from the generation elements to the network. If the power is augmented in the solar panels or wind turbine, the input current increases in the GSC.

The DC-link voltage tends to reach higher values, but in normal operation, the MSC's control increases the current reference and when the input and output power are the same, the systems reaches steady state. This way, the DC-link is the connection between the GSC and MSC: it is connected to a relatively high capacitance to absorb power oscillations during switching.

For security reasons, the system was designed with a braking chopper able to absorb an eventual power unbalance between the input and output. If the converter input power is higher than the output, the DC-link capacitors charge increasing the DC-link voltage. The braking chopper is activated if the voltage reaches excessive values, dissipating the extra energy in a resistance.

B. Photovoltaic Generation

Solar panels are made of *p-n* junction semiconductors designed in a thin layer that generate electric current when reached by solar radiation (photovoltaic effect). The energy from photons is captured by the electrons that change from a higher energy band layer in the semiconductor atoms, in this case, from the valence to the conduction band. The now "free" electrons move following the electric field created by the *p-n* junction, creating a current flow and generating energy.

This phenomenon has an intrinsic non-linear nature demanding specific operational conditions for an enhanced performance, since it provides a current-voltage and power-voltage non-linear relations (*I-V* and *P-V*) which depend on the solar radiation and cell's temperature. For this reason, maximum power point tracking (MPPT) algorithms are used for increasing the generated power in solar cells.

An equivalent model of a photovoltaic (PV) panel is presented in Fig. 3. It consists on a current source, an anti-parallel diode and two series and parallel resistances. This model is also known as five-parameter model and it adequately fits most of the modern PV panels in environmental situations close to the standard rating conditions (irradiation of 1000 W/m2 and cell temperature of 25(ºC)) [5].

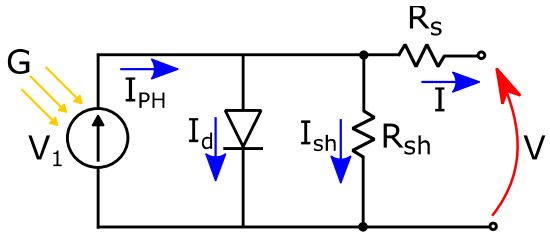

Fig. 3: Equivalent model of a photovoltaic panel.

The current source generates the photovoltaic current (I_{ph}), i.e. a current generated by the photovoltaic effect which is a function of the solar radiation and temperature. The cell output current (I) is defined in (1).

$$I = I_{PH} - I_d - I_{sh} \tag{1}$$

Where I_d is the diode current, I_{sh} is the current drained by the shunt resistor (R_{sh}) given by $I_{sh} = (V + I \cdot R_s)/R_{SH}$, with V the output voltage and R_s the series resistance. The diode current I_d is described in (2)

$$I_d = I_s \left[exp\left(\frac{q \cdot (V + I \cdot R_s)}{k \cdot T_c \cdot A} \right) - 1 \right] \tag{2}$$

The current I_s is the diode reverse saturation current, also known as leakage current; q is the charge of an electron ($q = 1.6 \cdot 10^{-19} C$); k is the Boltzmann's constant ($k = 1.38 \cdot 10^{-23}$J/K); T_c is the cell's temperature in Kelvin and A is the ideality factor and depends on the panel technology.

The saturation current (I_s) is expressed as shown in (3).

$$I_S = I_{RS} \cdot \left(\frac{T_c}{T_{Ref}}\right)^3 \cdot exp\left[\frac{q \cdot E_g \cdot \left(\frac{1}{T_{ref}} - \frac{1}{T_c}\right)}{k \cdot A}\right] \quad (3)$$

With I_{RS} is the reference reverse saturation current at a given temperature and solar radiation; E_g is the band-gap of the semiconductor.

Finally, with some simplifications we can express I_{RS} as written in (4).

$$I_{RS} = \frac{I_{sc}}{exp\left(\frac{q \cdot V_{OC}}{k \cdot A \cdot T_c}\right) - 1} \quad (4)$$

where I_{SC} is the short circuit current and V_{OC} is the open circuit voltage. Both parameters are often used for informing the electrical characteristics of the panel and most of the manufactures give these values in the component datasheet. The simplifications for arriving in (4) are ignoring I_d and I_{sh} during the short circuit test, that is to say, $I_{PH} = I_{SC}$.

Finally, all these equations permit an analysis of the panel characteristics as function of easily obtained parameters or constants. The TABLE I presents some electrical parameters of the photovoltaic panel model YL255P-29b from the manufacture *Yngli Solar*.

TABLE I: ELECTRIC PARAMETERS OF THE YL255P-29B,YNGLI SOLAR PANEL INFORMED BY THE MANUFACTURE.

Parameter	Symbol	Value
Module efficiency	η	*15.7%*
Voltage at P_{max}	V_{mpp}	*30.0(V)*
Current at P_{max}	I_{mpp}	*8,49(A)*
Open-circuit voltage	V_{OC}	*37.7(V)*
Short-circuit current	I_{SC}	*9.01(A)*

Using the above relations and the values in the TABLE I, the *I-V* curves of the YL255P-29b panels are shown in Fig. 4for different solar radiations.

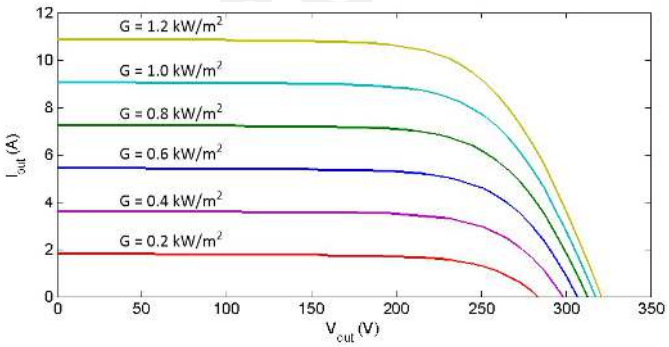

Fig. 4: Electrical characteristics of the panels YL255P-29b

C. Wind Power Generation

A *Darrieus-type* straight-bladed vertical axis turbine performs the wind generation of the HRGS. Vertical axis turbines are usually employed due to its simplicity since no yaw mechanism is required for orientation with the wind direction.

The straight-bladed turbines increase even more the mechanical simplicity of the system once the uniform section configuration is much easier to build, unlike the twisted and tampered blades often used in horizontal-axis or other vertical-axis turbines [6].

The major drawbacks of the *Darrieus* turbine are the operation in extreme conditions. During low speed, it presents inadequate or even negative torque which demands a relatively high wind conditions for the start-up. This reduces the operational range or even removes the possibility of self-starting and consequently reduces the system efficiency.

Beyond that, in high speeds, the turbine protection is compromised reducing the safety in this condition. These problems can be surmounted by changing the blades pitch angle, but this would make the turbine design and control more complex. For this reason, variable pitch blades turbines are unpractical for small scale and a fixed one is prioritized in this study.

The wind turbine used is a model Razek 266 (Fig. 5), from the Brazilian manufacturer ENERSUD, some characteristics given by the manufacturer are presented in TABLE II. This wind turbine has a spontaneous starting characteristic and was developed for use in inhabited locations, it combines the characteristics of low speed of rotation, low noise level and is suitable for operation with turbulent and variable direction winds.

Fig. 5: Wind turbine model Razek 266

The turbine's mechanical power, either vertical or horizontal, absorbed from the wind is given by (5) [7][8]

$$P_m = \frac{1}{2} C_p(\lambda) \rho A v^3 \quad (5)$$

where v and ρ are the wind speed and density, respectively; A is the sweep area covered and C_p is the turbine power coefficient that is provided by the manufacturer. The power coefficient is a

turbine aerodynamic characteristic that depends on the tip speed ratio (λ), expressed by $\lambda = \omega R/v$, with ω the angular velocity and R the turbine radius.

TABLE II: VERTICAL AXES TURBINE RAZEK 266 PARAMETERS

Parameter	Value
Nominal power	*1.5(kW)*
Rotor diameter	*2(m)*
Blades height	*2.66(m)*
Rotation starts at (wind speed)	*2,2(m/s)*
Generation starts at (wind speed)	*3,9(m/s)*
Nominal power at (wind speed)	*12(m/s)*
Weight	*110(kg)*

The turbine's power coefficient given by the manufacturer is presented in Fig. 6, the optimal C_p coefficient is obtained in λ = 1.6.

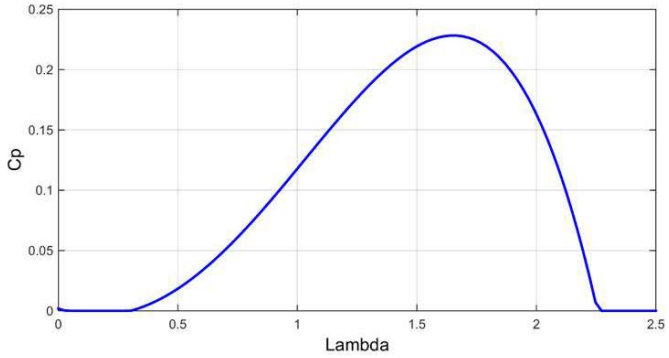

Fig. 6: Power curve of the Darrieus turbine Razek 266

The mechanical dynamics expressed in(6), where J is turbine's moment of inertia and B is the friction coefficient.

$$G_m = \frac{1}{Js + B} \tag{6}$$

The wind generation set Razek 266 uses a permanent magnet synchronous generator (PMSG), the direct and quadrature generator model of generator is written in (7) [8].

$$\begin{cases} v_{sd} = -R_s i_{sd} - \dfrac{d\lambda_{sd}}{dt} + \omega_e \lambda_{sq} \\ v_{sq} = -R_s i_{sq} - \dfrac{d\lambda_{sq}}{dt} - \omega_e \lambda_{sd} \end{cases} \tag{7}$$

where *Rs* is the stator resistance; ωe is the rotor electrical speed, v_S, i_S and λs are the stator voltage, current and flux, respectively. According to the adopted orientation, the *d*-axis reference frame is aligned with the flux of the magnets (ψ_m). The stator linkage fluxes decomposed in *dq*-axes expressed as $\lambda_{sd} = L_{sd} i_{sd} + \psi_m$ and $\lambda_{sq} = L_{sq} i_{sq}$ with L_{sd} is the stator inductance in the direct axis and L_{sq} in the quadrature.

The electrical torque (T_e) is a function of the fluxes and currents interaction and the number of poles (n_p) in the machine as shown in (8).

$$T_e = \frac{3}{2} n_p \left[\lambda_{sd} i_q - \lambda_{sq} i_d\right] \tag{8}$$

D. Parallel Interleaved Boost Converters

The generation side converter is constituted of three interleaved boost converters (B1, B2 and B3) independently controlled. Two of these converters are connected to the two solar panels arrays and the third one is connected to the rectifier of the wind generator. The photovoltaic boost converters are connected to LC filters and the wind boost converter to a single inductor, as shown in Fig. 1.

In this work, was used the technique proposed in [9], where it is made the use of the interleaved Boost converter for multiple inputs with the same output. The cells interleaving requires that they are operating at the same switching frequency, but with a phase displaced from the other of *360° / N*, where *N* is the number of cells, this operation produces an increase of (*N*) times in the frequency of the ripple of Output and a ripple reduction of the output current by a factor (*N*) [10].

The output currents are the sum of the diode currents, its output frequency is twice higher than the switching frequency in addition to a ripple reduction that implies a smaller output capacitor, reduced filters and losses, the best instant of ripple reduction occurs for duty cycle of 50% [11]

The steps for the boost parameters design are described as follows.

- Defining the desired boost ripple (ΔI_{BC}) and consequently the component's inductance (L) as a function of the input and DC-link voltages (Vi, VDC) and the switching frequency (fs), as presented in(9).

$$L = \frac{V_i (V_{DC} - V_i)}{2\pi f_s \Delta I_{BC} V_{DC}} \tag{9}$$

- Defining the input capacitance for reducing the ripple in the solar panels in order to keep high efficiency. For the wind generator, this step is not required. The capacitance required depends on the cell's desired output voltage ripple (ΔV_{PV})., the array total power and voltage (P_{PV}, V_{PV}) and switching frequency as (10).

$$C = \frac{P_{PV}}{2\pi f_s \Delta V_{PV} V_{PV}} \tag{10}$$

In what concerns the inductor ripple, it is important not to have high values for reducing the inductor and converter losses, working in continuous current mode. In the other hand, a very low ripple would demand a high inductor increasing the system's cost and size. A current ripple value of 7% was adopted for calculating the boost inductance in the PV boosts. For simplification, the same inductance was used in the wind generator boost and a similar absolute ripple will be presented in the circuit.

In order to accomplish that, an inductor of 1.5(mH) was used. Since the nominal photovoltaic and wind generator's voltage are similar (300(V) and 311(V),respectively), similar current ripples will be present in DC-DC converters: 1.25 in the

PV circuit and 1.27 in the wind circuit. It is important to notice that the ripple percentages are very different due to the sources' power variation: 7% current ripple in the photovoltaic circuits (of 5(kW) each) and 30% in the wind generator circuit (of1.5 (kW)).

For defining the boosts input capacitance, the panel's voltage/current desired ripple is the parameters to be analyzed. As already mentioned, in order to operate in maximum power, a specific voltage might be applied to the solar array for each irradiation. Once a boost converter is used for stepping-up the panel output voltage, a high frequency component will be present in this variable. The voltage ripple reduces the generated power since the oscillations vary the maximum power voltage (V_{mpp}) allowing the panel to operate with lower efficiency. In[12], it is shown that in order to keep the utilization ratio in 98%, the voltage ripple should be below 8.5% of the V_{mpp}. The efficiency is lower, 95% for the same ripple in the study presented in [13]. The authors results are even more restrict in [13] presenting a 2.7% and 6.83% power reduction with ripples equal to 5% and 8% respectively.

This latter study emphasizes that under variations in the irradiance, the losses can be significantly higher than the number presented. These differences obtained in the different studies are justified by the dependence on the cells' characteristics and on the MPPT algorithm adopted. In the generation system design, a conservative voltage ripple of 2% was adopted in the system design. Although this component is the main limiting in what concerns the system lifetime [12], in order not to use a bulky inductor, a capacitor of 450µF was adopted in the panel output.

III. Experimental Set-Up

The conversion system is constituted by two Semikron Stacks (converters) model B6CI+B1CI+B6U. Each stack has four half-bridges (IGBT model SKM100GB12T4), a non-controlled rectifier, driver and snubber circuits, DC-link capacitance and balance resistors. One stack is the Mains Side Converter (MSC) and the second is the Generation Side Converter (GSC).

A DSP model TMS320F28335 from Texas Instruments performs the control. The Fig. 7 presents the converter cabinet.

Fig. 7: Converter cabinet of the HRGS.

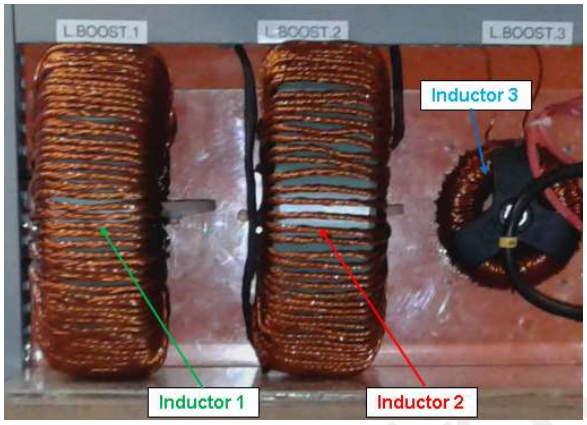

Fig. 8: Boost inductors

The Fig. 8 shows the designed boost inductors manufactured by the authors. The TABLE III describe the generator side components.

TABLE III: Generator Side Converter Components

System overall Power		*11.7 KW*
Photovoltaic generation	Nominal power	*10.2 KW*
	Number of cells	*40*
	Number of arrays	*4*
	Nominal array voltage	*300V*
	Nominal array current	*8.49A*
Wind generation	Nominal power	*1.5 KW*
	Nominal voltage	*220V*
	Number of phases	*3*
DC link	DC-link Operational voltage	*450V*
	DC-link Capacitance	*9400µF*
	Chopper Resistance	*100Ω*
Generation Side Converter (GSC)	Switching Frequency	*10,08kHz*
	Nominal Input Voltage B1 and B2	*300V*
	Nominal Input Current B1 and B2	*8,49A*
	Nominal Input Voltage B3	*311V*
	Nominal Input Current B 3	*4,82A*

IV. Identification of System'sparameters

A. Photovoltaic Panels Identification

In order to confirm and refine the solar panels' characteristics, the PV analyzer model PVA-600 from the manufacturer *Solmetric* accomplished some measurements. This instrument measures and traces the panel's "*I versus V*" and "*P versus V*". To obtain these curves, the instrument measures not only the electrical variables (panel's voltage and current), but also the irradiance and the cells' backside temperature.

The measurements of panels' variables are important for refining the parameters given by the manufacturer and also for finding the values that are not available, like the series and parallel resistances. Fig. 9 presents the comparison between

measured and simulated data after the identification, in order to validate the model.

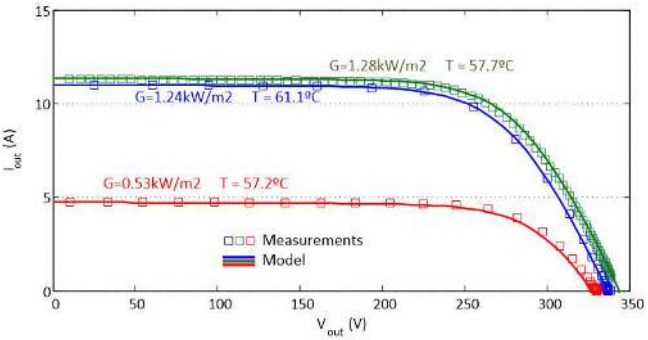

Fig. 9: PV Model validation with the measured data

The results show an important similarity corroborating to the good quality of the model. The parameters obtained from the system identification are presented in TABLE IV.

TABLE IV: PANEL'S ELECTRIC PARAMETERS DERIVED FROM THE PV ANALYZER DATA.

Parameter	Symbol	Value
Series resistance	R_s	*0.35(Ω)*
Parallel resistance	R_p	*286.9(Ω)*
Temperature coefficient (in Volts per Kelvin)	α_{PV}	*0.06(%/ºC)*
Open-circuit voltage	V_{OC}	*39.58(V)*
Short-circuit current	I_{SC}	*9.01(A)*

B. *Wind turbine mechanical dynamics identification*

In order to define the turbine's moment of inertia (J) and friction coefficient (B), a simple test should be performed that consists on imposing a torque, which drives the system to a certain speed, removing the input torque and getting the slowdown curve. If there is no speed measurement, this curve can be obtained from the induced voltage (proportional to the speed, number of poles and the fixed flux from magnets).

Although the electrical frequency decays linearly with the mechanical speed, the voltages presented in Fig. 10does not present this characteristic. The reason for that is the aliasing effect derived from the high sampling period (200(ms)) required for recording a long period in a standard oscilloscope (TPS2000 from Tektronix). Despite the aliasing effect, the peak voltage decay could be registered allowing the system identification. TABLE V presents the parameters obtained from the slow-down curve.

TABLE V: TURBINE'S MECHANICAL DYNAMICAL PARAMETERS

Parameter	Symbol	Value
Moment of inertia	J	*45(kg.m²)*
Friction coefficient	B	0.34 (N.m.s)
Mechanical time constant	τ_m	132 s

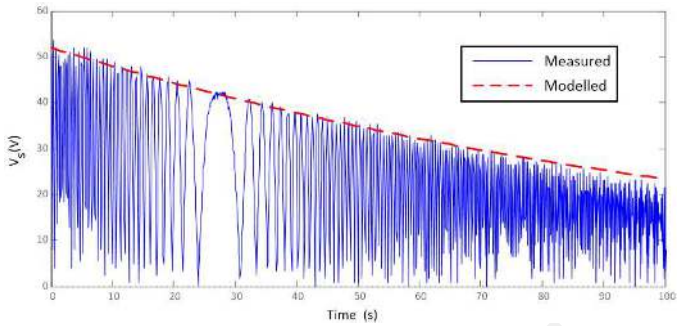

Fig. 10: Slow-down induced stator voltage

C. *PMSG Identification*

From the dynamics equations PMSG the stator resistance (R_S), magnets' flux (ψ_m), and dq-inductances (L_d and L_q) must be identified or measured.

To find the magnets' flux, from equation (7) and stator linkage fluxes expressions, it is possible to notice that the induced voltage only depends on the magnets' flux and stator electrical frequency.

During open circuit tests, the internal induced voltage is presents in the stator terminals, since there is no voltage drop in the stator impedance. So the flux was calculated based on the equation(11), during the machine open circuit test, only the q component of the stator voltage is presented.

$$\psi_m = \frac{-v_{sq}}{\omega_e} \qquad (11)$$

For the mechanical characteristics of the rotor, some saliency is expected due the rotor non-cylindrical aspect, thus, when the rotor flux is aligned with the stator polarity (*d-axis*), the inductance is lower since the position of the magnets increases the flux reluctance.

The inverse effect happens when the rotor position is shifted by 90º with respect to the stator. In order to measure this difference, the rotor position should be known and fixed. This way, the measurement of the dq-inductance was accomplished following the steps below.

- Connect the phases B and C and apply a DC voltage between phases $A(+)$ and $BC(-)$(Fig. 11(a));
- Align the rotor with the stator resultant flux (d axis) and lock the rotor;
- Apply a voltage step with negative pole in the phase A and positive in the connection BC, measure the current response dynamics (defined by L_d and R_s),
- Remove the connection and apply a DC voltage between phases C and B leaving phase A opened (Fig. 11(b)).
- Align the rotor with the stator resultant flux and lock the rotor; the new position will be shifted 90º electrical degrees from the first position (q axis),
- Return to the first connection and apply a voltage step, but now, with positive pole in the phase A and negative

in the connection *BC*, measure the current response dynamics (defined by L_q and R_s),

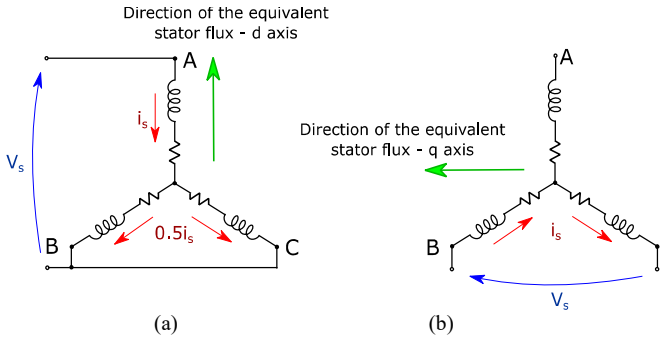

(a) (b)

Fig. 11: Configuration for the dq alignment. (a) For measuring the d-axis impedance (b) For measuring q-axis impedance.

A current sensor A622 and an oscilloscope TPS2000 and passive voltage probes, all from Tektronix, accomplished the measurements. Fig. 12presents the step applied to the stator winding (yellow CH1) and the current response (blue CH2) for the *dq* inductances measurements. The identified PMSG electrical parameters are presented in TABLE VI.

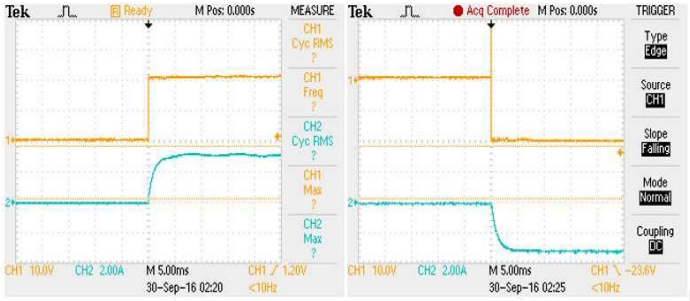

(a) (b)

Fig. 12: Step tests for defining dq-axis inductance: the stator voltages and currents are presented in yellow (CH1) and blue (CH2), respectively. (a) the d-axis is shown and in (b) the *q*-axis.

TABLE VI: MECHANICAL DYNAMIC PARAMETERS OF THE TURBINE.

Parameter	Symbol	Value
Direct axis inductance	L_d	*11.5(mH)*
Quadrature axis inductance	L_q	*11.7(mH)*
Stator resistance	*Rs*	*16.7(Ω)*
Pair of poles	n_p	*18*
Magnets flux	ψ_m	*0.79(V.s)*

D. *Boosts' Filter Identification*

The boost LC model (G_b) can be represented by the transfer function presented in (12).

$$G_b = \frac{C_b s}{L_b C_b s^2 + R_b C_b s + 1} \tag{12}$$

Where L_b, C_b and R_b are the boost inductance, capacitance and resistance, respectively. For the system parameters identification, was measured the filter inductance using a LCR meter model UC1751C from Agilent and resistance using a low resistance meter MR-10W from Eletroteste. The founded values are in the TABLE VII.

TABLE VII: BOOST INDUCTORS MEASURED VALUES

Parameter	Symbol	Value
Boost 1 inductance	L_1	*2,71mH*
Boost 1 resistance	R_1	*71mΩ*
Boost 2 inductance	L_3	*2,71mH*
Boost 2 resistance	R_2	*68mΩ*
Boost 3 inductance	L_3	*2,6mH*
Boost 3 resistance	R_3	*182mΩ*

V. EXPERIMENTAL RESULTS

In this section, will be discussed the practical results obtained in steady state, since the control dynamics is not the focus of this paper.

A. *Photovoltaic generation*

Fig. 13(a) shows the current ripple of the first (purple CH3) and second (green CH4) boost converter, where the current ripple was around 4.8(A).

Fig. 13(b) shows the current ripple of the first boost converter (purple CH3) and in the first panel array (green CH4). The panel array presets a current ripple around 0.8(A), which demonstrates how the interleaved boosts techniques reduce current ripple into the panels array.

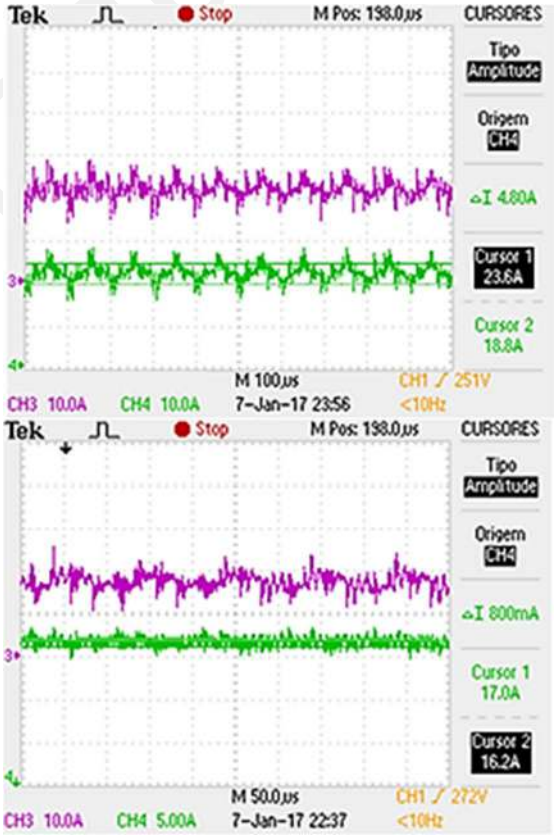

Fig. 13: (a) Current ripple of the first (purple CH3) and second (green CH4) boost converter (b) current ripple of the first boost converter (purple CH3) and in the first panel array (green CH4).

B. *Wind generation*

Fig. 14 shows the PMSG currents in nominal power where the low order harmonics generated by the rectification can be observed.

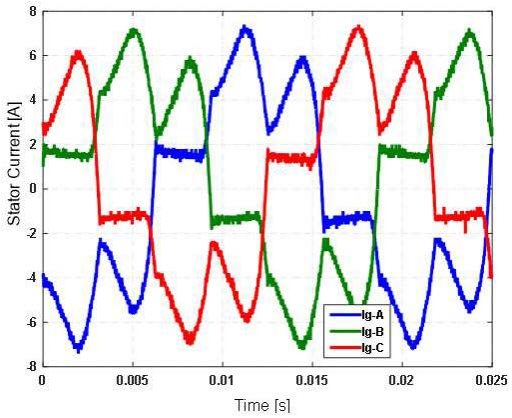

Fig. 14: Generator currents in nominal operation

Fig. 15shows the input voltage (Fig. 15(a)) and current (Fig. 15(b)) at the boost converter and the instantaneous power (Fig. 15(c)). It is verified that at nominal speed the average power delivered by the wind turbine was approximately 1450 VA.

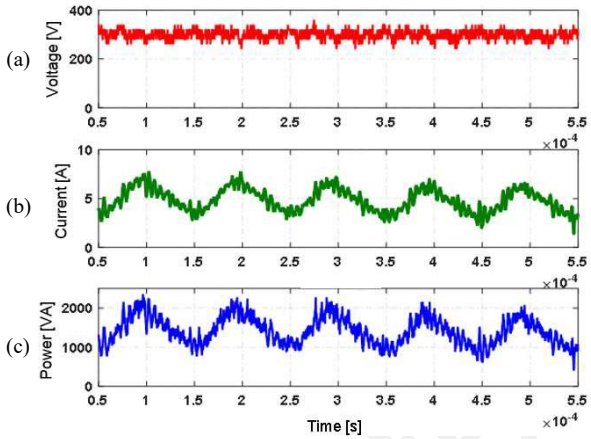

Fig. 15: input voltage (a) current (b) and the instantaneous power(c) at the PMSG Boost converter

CONCLUSIONS

The present study presented the design of generation side converter of an 11.7KW photovoltaic/wind HRGS. The generation elements are the solar panels, wind turbine and PMSG. After these elements are chosen for the HRGS, the conversion topology must be chosen and the design accomplished. The power sources are connected to boost converters (GSC) which are linked to a 4-cell VSI (MSC) through a DC-link. The design of GSC was approached as well as their modeling and parameter identification. For the proper simulation and operation, all the dynamics to be controlled must be identified with measurements for guarantying similarity to the real system.

ACKNOWLEDGMENT

The authors thank Prof. Clodualdo Sousa and all the members of the Conversion and Control of Electric Energy - CCEE Research Group at UNIFEI, *Campus* Itabira.

This work has been supported by the Brazilian agencies CAPES and CNPq.

REFERENCES

[1] N. A. Ahmed, M. Miyatake, e A. K. Al-Othman, "Power fluctuations suppression of stand-alone hybrid generation combining solar photovoltaic/wind turbine and fuel cell systems", Energy Convers. Manag., vol. 49, no 10, p. 2711–2719, out. 2008.

[2] HAMATWI, E.; DAVIDSON, I. E. Optimised Model of a Solar/Wind/Diesel Hybrid Generation System for Rural Application. future, v. 7, p. 8.

[3] STURDIVANT, Rick; CHONG, Edwin KP. Systems Engineering of Hybrid Renewable Electric Power. In: 2016 IEEE Green Technologies Conference (GreenTech). IEEE, 2016. p. 90-94.

[4] HAMATWI, Ester et al. Model of a hybrid distributed generation system for a DC nano-grid. In: 2016 Clemson University Power Systems Conference (PSC). IEEE, 2016. p. 1-8.

[5] V. Lo Brano, A. Orioli, G. Ciulla, e A. Di Gangi, "An improved five-parameter model for photovoltaic modules", *Sol. Energy Mater. Sol. Cells*, vol. 94, nº 8, p. 1358–1370, ago. 2010.

[6] M. Islam, D. Ting, e A. Fartaj, "Aerodynamic models for Darrieus-type straight-bladed vertical axis wind turbines", *Renew. Sustain. Energy Rev.*, vol. 12, nº 4, p. 1087–1109, maio 2008.

[7] KIM, Seul-Ki et al. Dynamic modeling and control of a grid-connected hybrid generation system with versatile power transfer. IEEE transactions on industrial electronics, v. 55, n. 4, p. 1677-1688, 2008.

[8] KENDECK, C. Ndjewel; RAJI, Atanda K. Control of permanent magnet synchronous generator based wind turbine and fault ride-through improvement during faulty grid conditions. In: Industrial and Commercial Use of Energy (ICUE), 2016 International Conference on the. IEEE, 2016. p. 298-304.

[9] HU, Boyang; SATHIAKUMAR, Swamidoss. Current *ripple* cancellation of multiple paralleled *Boost* converters for pv/battery charging system with mppt. In: Innovative Smart Grid Technologies Asia (ISGT), 2011 IEEE PES. IEEE, 2011. p. 1-6.

[10] ASSUNÇÃO, M. R. "Estudo e implementação de um conversor CC-CC *Boost* entrelaçado em regime de condução contínua" - Dissertação de Mestrado -Área de pesquisa: Eletrônica de Potência, PPGEE - UFMG, 2014.

[11] AMUDHAVALLI, D. et al. Interleaved soft switching *Boost* converter with MPPT for photovoltaic power generation system. In: Information Communication and Embedded Systems (ICICES), 2013 International Conference on. IEEE, 2013. p. 1214-1219.

[12] S. B. Kjaer, J. K. Pedersen, e F. Blaabjerg, "A Review of Single-Phase Grid-Connected Inverters for Photovoltaic Modules", IEEE Trans. Ind. Appl., vol. 41, no 5, p. 1292–1306, set. 2005.

[13] C. R. Sullivan, J. J. Awerbuch, e A. M. Latham, "Decrease in Photovoltaic Power Output from Ripple: Simple General Calculation and the Effect of Partial Shading", IEEE Trans. Power Electron., vol. 28, no 2, p. 740–747, fev. 2013.